the validity of eqn. 2. A sinusoidal dither current of 127 mA RMS was applied to the loudspeaker at a frequency of 325 Hz. With zero mean lateral displacement of the fibre this

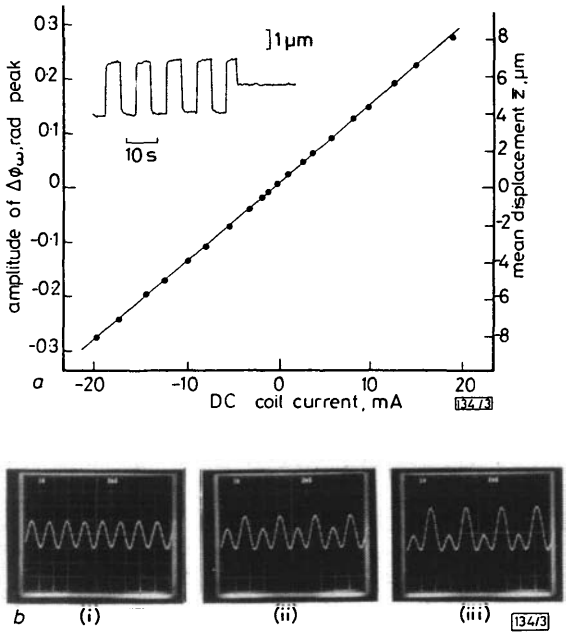

Fig. 3 *Experimental results*

a Amplitude of the phase shift component at the fundamental (dither) frequency with DC coil current. The right-hand ordinate shows the mean displacement calculated from eqn. 2. Inset shows a typical LIA output response to a $\pm 1{\cdot}4$ μm square-wave displacement at 0·1 Hz ($\tau_{LIA} = 30$ ms)

b Oscilloscope recordings showing the interferometer phase shift (compensator feedback voltage) for three displacements: (i) zero, (ii) 10 μm and (iii) 20 μm

generated an interferometer phase shift of $\Delta\phi_{2\omega} = 0{\cdot}48$ rad peak, corresponding to a dither amplitude $z_0 = 52$ μm. The mean displacement of the centre of the fibre was then varied via control of the DC current supplied to the loudspeaker coil, and the amplitude $\Delta\phi_\omega$ of the phase shift component generated at the fundamental (dither) frequency ω was recorded. Eqn. 2 was then used to determine the actual fibre displacement $\bar{z}$. The results of this experiment are plotted in Fig. 3*a*, from which a displacement responsivity of 0·4 μm/mA can be determined for the loudspeaker. The oscilloscope photographs of Fig. 3*b* show the induced phase waveform observed for three mean displacements, and demonstrate the change in the harmonic content of $\Delta\phi$ with $\bar{z}$; the increasing amplitude of $\Delta\phi_\omega$ with displacement is clearly evidenced by these photographs.

The minimum detectable displacement $\bar{z}_{min}$ is determined by the interferometer phase shift noise floor $\Delta\phi_{min}$ at the dither frequency, the amplitude of the dither z_0 and the dimensions of the system through eqn. 2; thus $\bar{z}_{min} = \Delta\phi_{min}\lambda d/4\pi n\xi z_0$. In our experimental system, phase noise generated by laser frequency jitter produced a $\Delta\phi_{min}$ of $\sim 1{\cdot}5 \times 10^{-5}$ rad $Hz^{-1/2}$ at ~ 300 Hz, which for a dither amplitude $\simeq 50$ μm peak ($z_0/d \sim 0{\cdot}002$) gives $\bar{z}_{min} = 4 \times 10^{-10}$ m (4 Å). This is a very respectable displacement sensitivity, which could be improved by an order of magnitude simply by improving the phase detection sensitivity of the interferometer (i.e. to $\sim 10^{-6}$ rad $Hz^{-1/2}$). In general, this sensitivity cannot be surpassed using conventional linear straining of optical fibre in an interferometric system. We feel, therefore, that this phase transduction technique will have a strong impact on the design of interferometric sensors for DC measurands such as acceleration, pressure and possibly electric field sensors. Experimental tests of an accelerometer based on this technique are currently in progress in our laboratories and will be reported later.

In conclusion, we have described and demonstrated the feasibility of a new nonlinear phase transduction method for use with DC measurand interferometric fibre sensors. The technique can be utilised in the development of true DC sensors for the measurement of displacement, acceleration, pressure and other measurands. A minimum detectable displacement of 4×10^{-10} m has been demonstrated at DC.

A. KERSEY*
F. BUCHOLTZ
A. DANDRIDGE

Naval Research Laboratory
Washington, DC 20375-5000, USA

* Sachs Freeman Associates, Landover, MD 20785, USA

25th November 1985

References

1 GIALLORENZI, T. G., BUCARO, J. A., DANDRIDGE, A., SIGEL, G. H., JUN., COLE, J. H., RASHLEIGH, S. C., and PRIEST, R. G.: 'Optical fibre sensor technology', *IEEE J. Quantum Electron.*, 1982, **QE-18**, pp. 626–664

2 See, for example: Proceedings of 2nd international conference on optical fibre sensors, September 1984, Stuttgart (VDE Verlag GmbH, 1984)

3 KOO, K. P., DANDRIDGE, A., TVETEN, A. B., and SIGEL, G. H., JUN.: 'A fibre-optic DC magnetometer', *IEEE J. Lightwave Technol.*, 1983, **LT-1**, pp. 524–525

4 KERSEY, A. D., CORKE, M., JACKSON, D. A., and JONES, J. D. C.: 'Detection of DC and low-frequency AC magnetic fields using an all single-mode fibre magnetometer', *Electron. Lett.*, 1983, **19**, pp. 469–471

5 KOO, K. P., and SIGEL, G. H., JUN.: 'Detection scheme in a fibre-optic magnetic-field sensor free from ambiguity due to material magnetic hysteresis', *Opt. Lett.*, 1984, **9**, pp. 257–259

6 KERSEY, A. D., JACKSON, D. A., and CORKE, M.: 'Single-mode fibre-optic magnetometer with DC bias field stabilization', *IEEE J. Lightwave Technol.*, 1985, **LT-3**, pp. 836–840

7 BUTTER, C. D., and HOCKER, G. B.: 'Fibre optic strain gauge', *Appl. Opt.*, 1978, **17**, pp. 2867–2869

COMPENSATION OF SAW FILTERS BY EXPERIMENTAL PERTURBATION OF IDTS

Indexing terms: Ultrasonics, Surface-acoustic-wave devices, Transducers

A SAW bandpass filter on (*YZ*) $LiNbO_3$ with two apodised transducers and a multistrip coupler is compensated in its rejection response from an initial 52 dB level to a 64 dB level. The compensation is accomplished through a technique that determines filter sensitivity through measurements of change in filter electrical response to perturbations in electrode length.

In previous results[1,2] it was demonstrated that surface-acoustic-wave (SAW) bandpass filters could be compensated by an *in situ* perturbation procedure. Incremental shortening of individual electrodes in the interdigitated transducer (IDT) was used to determine the sensitivity of the filter frequency response to such perturbations. These data allowed us to predict and implement a modified apodisation which reduced its overall sidelobe level from 28 dB to 39 dB. This filter consisted an apodised input transducer, a multistrip coupler (MSC) and a broadband three-wavelength output transducer. Greater rejection is achieved from the typical arrangement of weighted input transducer, MSC and weighted output transducer. While lower sidelobe levels increase the uncertainty of filter response measurements due to noise and spurious effects, improvement through compensation is still possible. Starting with a filter with sidelobes at a 52 dB level, it was possible to compensate the response to a general level of 70 dB with one sidelobe at 64 dB.

The specific filter designed and compensated was fabricated on (*YZ*) $LiNbO_3$. The centre frequency wavelength λ_0 was 36·6 μm, which resulted in a 94 MHz centre frequency. The filter, shown in Fig. 1, consisted of a 138-strip multistrip coupler (MSC) and two apodised transducers, each with 31 double-electrode transducers, which were identical to the apodised transducer of the compensated filter discussed above.

The aperture of each transducer measured 167 λ_0. The aperture of the MSC was 365 λ_0 and the stripes and spaces were both $\lambda_0/8$. The device was mounted on a metal header and the

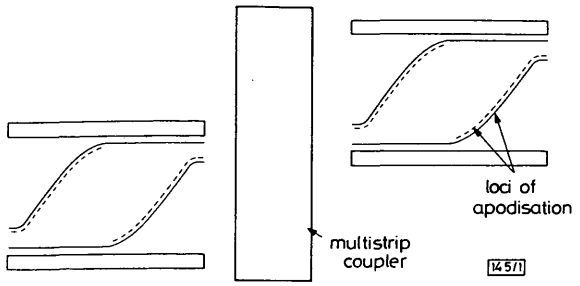

Fig. 1 *Filter layout*

input and output transducers were ball-bonded with 1 mm gold wire directly into a 50 Ω transmission measurement system. No intermediate circuit elements were included to impedance-match the electric ports. This device, although employing an MSC, still showed evidence of bulk mode corruption below midband at 65 to 70 dB levels. After sandblasting the backside of the crystal, the sidelobes had a more regular appearance (as displayed by the unshaded curve in Fig. 2).

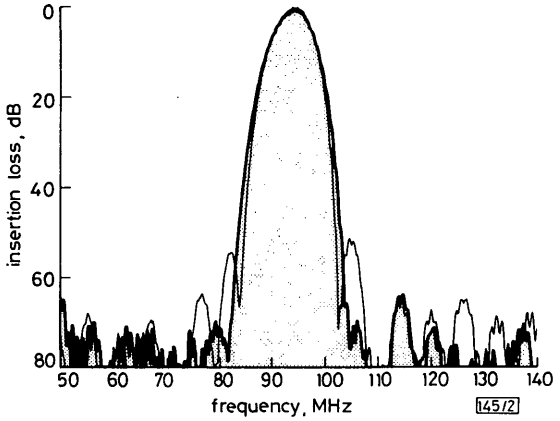

Fig. 2 *Filter response before (unshaded) and after (shaded) compensation*

Filter insertion loss is approximately 16 dB

The filter response was perturbed by scribing a 5 λ_0 length off the end of a double-electrode using a Micromanipulator 6000 micropositioning scribe.† The transmission response of the filter before and after perturbation was measured with a phase-locked HP8507 automatic network analyser (ANA) from 44 to 144 MHz at 545 frequencies. The difference between the two complex-valued measurements gives the sensitivity to the electrode length filter perturbation, which we refer to as the 'perturbation measurement'. A set of perturbation measurements is gathered and supplied to a computer program which computes an optimal correction required for a desired response. The predicted electrode length modifications are implemented manually as in the case of the original perturbations. Amplifiers were used before and after the filter to reduce noise due to the filter's extreme loss in the sidelobe region. A 21 dB preamplifier brought the device input power to ~23 dBm. Greater input levels led to noticeable phase shifts through device heating. Additional postamplification of 25 dB improved repeatability, but to a smaller degree. This high gain caused saturation of the ANA detectors in the device passband. The saturated portion of the frequency range was excluded from the measurements and was not required for the intended purpose of sidelobe reduction.

For the purpose of testing the *in situ* techniques, an efficient compensation algorithm with few complicating assumptions was sought. With the assumptions that perturbations to the electrodes produce frequency response changes that are independent of one another and that the changes are linearly proportional to the length of trim, an exact algorithm with a linear solution is possible. Furthermore, if these assumptions are only approximately true, the algorithm could still converge through iteration. Thus, an approximate linear model of the perturbation dependence on electrode trim is preferred to an exact nonlinear model, which requires a larger set of measurements for parameterisation and a numerically intensive solution. Least-squares problems can be specified whose solutions satisfy these conditions.

The compensation algorithm specifies modifications to the uncorrected apodisation by choosing N optimal electrode length modifications $\hat{a}_i$, which when multiplied by the perturbation measurements $T_i(f)$ give the best approximation in a least-square sense to $y(f)$, where $y(f)$ is the difference between the desired and uncorrected frequency responses. In addition, a Lagrange multiplier γ was included to impose a constraint minimising the total change allowed to the filter electrode lengths. In this way small perturbations can be used that have relatively linear effects and convergence can be achieved in a few steps.

A cost function with a linear solution for the optimum coefficients, given by

$$J = \sum_f \left\{ \left(\sum_{i=1}^{N} a_i T_i - y \right) \left(\sum_{i=1}^{N} a_i T_i - y \right)^* W + \gamma \sum_{i=1}^{N} (a_i T_i (a_i T_i)^* \right\} \quad (1)$$

was chosen, where $W(f)$ is a set of weights emphasising in which portions of the frequency response more improvement is desired.

Minimisation of the mean-square error is achieved by setting the partial derivatives with respect to each coefficient a_i to zero. The resulting linear equations are solved for $\hat{a}$ (optimum a) by inversion of a matrix. The optimum filter response is then

$$\hat{H} = H + \sum_{i=1}^{N} \hat{a}_i T_i \quad (2)$$

where positive a_i indicates a shortened overlap if $T_i(f)$ was found through a shortening operation.

Although the algorithm as described is noniterative, it was necessary to modify γ and the weighting function $W(f)$, and set added constraints on some of the scaling coefficients a_i. Since electrode overlaps can only be shortened using our device perturbation procedure, negative values for a_i could not be implemented. When negative values were found for a_i, the corresponding $T_i(f)$ was removed from consideration (i.e. $a_i = 0$) and the filter response was reoptimised.

The desired frequency response supplied in calculating the uncompensated filter error $y(f)$ was chosen to be zero out of band (i.e. the lowest sidelobe levels are desired), and weighting $W(f)$ was chosen to be zero inband so that all optimisation effort was directed towards sidelobe improvement. In this procedure, under operator control, $W(f)$ was modified to increase emphasis on certain sidelobes that were higher than others; nonpositive a_i were set to zero and γ was chosen to limit extreme variations in tap weight. By modifying the above variables, reasonable improvement may be found in about 10 iterations of the calculations. These calculations can be made in 2 h, with nearly all of the time spent in operator review of program output and not in computer CPU time.

After implementing the new tap weights the filter is remeasured and a new set of additional scale factors are derived after replacing H (in eqns. 1 and 2) with the new filter response measurement. These new $\hat{a}_i$ lead to further improvement in the filter response, as long as the algorithm predicts some positive scale factors and the original perturbation measurements continue to approximately describe filter sensitivity (i.e. the original perturbation measurements $T_i(f)$ continue to be valid for the perturbed filter).

The filter was compensated in three iterations. A database of 16 perturbation measurements was gathered by perturbing alternate double electrodes for the first rransducer, and one cycle of compensation was performed on this transducer. Then another database of 16 perturbation measurements was

† Micromanipulator Co., 1100 Corbett Street, Carson City, NV 89701, USA

gathered for the second transducer, and two cycles of compensation were performed. The filter sidelobes were improved from 52 to 64 dB (Fig. 2). The high-frequency sidelobe at the 64 dB level sets the limit to sidelobe performance. It was discovered through simulation that the side could be further lowered but to the detriment of a complementary sidelobe below the passband. Except for this sidelobe, the general rejection level is ~70 dB to the edges of the weighted frequency range 44 to 144 MHz.

One possible modification to the above procedure for compensation that has not been tried would be to perturb both apodised transducers and then optimise with respect to all trims on both transducers. Care should be taken to make these perturbations small, since we observed a large change in the perturbation measurement envelopes between the first and second transducer perturbations. Enhanced sidelobe levels noted of the perturbation measurements in the second learning set lead us to believe that the first transducer was overcompensated during the course of these sequential optimisations. This would not have occurred if simultaneous optimisation of both transducers had been carried out.

In compensating a filter with apodised input and output to 64 to 70 dB levels over a 100% bandwidth, we have shown that *in situ* compensation is practical for SAW filter development in extending the performance limits of filters which depend on the apodisation of both transducers. It is felt that *in situ* compensation procedures could be fully automated and in such a format become a design tool that would accelerate development of high-performance filters.

R. W. COHN
R. S. WAGERS*

Texas Instruments Incorporated
Central Research Laboratories
Dallas, TX 75265, USA

27th November 1985

* Current address: Fisher Controls, 1712 Centre Creek Drive, Austin, TX 78754, USA

References

1 COHN, R. W., and WAGERS, R. S.: '*In situ* compensation of SAW filter response', *Appl. Phys. Lett.*, 1985, **47**
2 WAGERS, R. S., and COHN, R. W.: 'Residual bulk mode levels in *(YXI) 128°* $LiNbO_3$', *IEEE Trans.*, 1984, **SU-31**, pp. 168–174

ENDLESSLY ROTATABLE FRACTIONAL-WAVE DEVICES FOR SINGLE-MODE-FIBRE OPTICS

Indexing terms: Optics, Fibre optics

Endlessly rotatable fractional-wave devices for polarisation control in single-mode fibres are described which utilise stress birefringence induced by fibre bending, and are free from fibre twist by rotating the fibre around its own axis. Experiments confirm that these devices rotate endlessly and have small hysteresis.

Introduction: Polarisation devices in fibre optics are researched from various viewpoints. For multimode fibres, in which the polarisation state is random at a transverse section, micro-optic devices with polarisation-independent characteristics have been researched.[1] For single-mode fibres, in which two orthogonally polarised modes exist in general, devices such as polarisation controllers, polarisation dividers, polarisation-preserving fibres etc. have been studied and fabricated.[2–4]

All-fibre devices have the advantage of low-loss characteristics. However, single-mode fibre-optic polarisation controllers reported thus far have a problem in that their birefringence principal axes cannot be endlessly rotated.[2–3] This is because rotations may cause fibre twist or require the increase of supplied voltage or current.

The endless rotation function in polarisation controllers is particularly important in a coherent detection of optical fibre transmission.[5,6] This letter describes new single-mode fibre-optic fractional-wave devices, by which polarisation controllers having an endless-rotation function can be constructed. Our study is independent of the work on rotatable fibre cranks recently reported by T. Okoshi *et al.*[7]

Configuration: In the conventional device proposed by Lefevre,[3] as a fibre is wound and fixed on a bobbin, the fibre can be considered as fixed on an imaginary plane which is transverse to the bobbin axis. Accordingly, rotation of the bobbin, or rotation of the imaginary plane, causes fibre twist. Schematic representations of the endlessly rotatable fractional-wave devices are shown in Figs. 1 and 2. In the

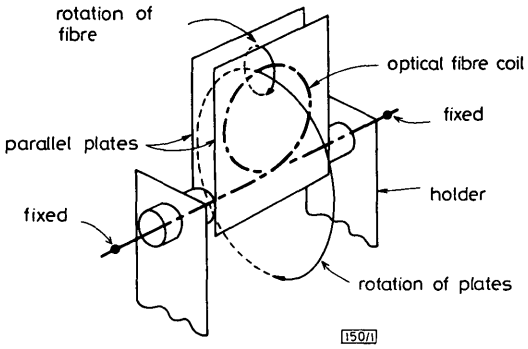

Fig. 1 *Endlessly rotatable fractional-wave device (I)*

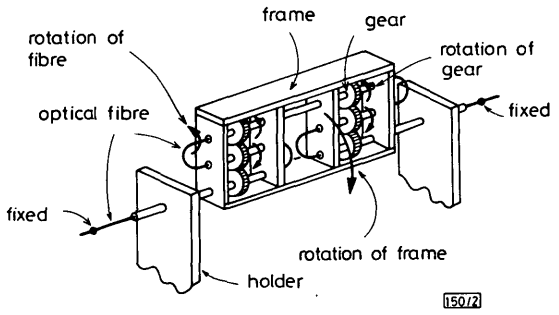

Fig. 2 *Endlessly rotatable fractional-wave device (II)*

same manner as the conventional device, birefringence of each device is induced by bending the single-mode fibre along an imaginary plane. The imaginary planes in Figs. 1 and 2 correspond to the space between the parallel plates and the frame, respectively. Rotation of the imaginary planes causes the birefringence principal axes to rotate without any fibre twist. This is because the fibres rotate simultaneously around their own axes with respect to the imaginary planes.

The devices in Figs. 1 and 2 use different mechanisms for the fibre rotation. In Fig. 1, the fibre is bent into a coil, and is inserted between two parallel rotatable plates to be loosely supported therein. If the effects of fibre-to-fibre and fibre-to-plate frictions are small in the rotated plates, the fibre therein can rotate spontaneously around its own axis owing to its shear stress. In Fig. 2, the fibre is inserted into the six gears supported by a rotatable frame. Since four semicircular bends are formed in the fibre, birefringence of the device corresponds to that of a two-turn fibre coil. The two gears on the rotation axis of the frame are fixed to the holders so as not to rotate. With the rotation of the frame, other gears change their positions along concentric circles, and rotate the fibre therein around its own axis without any twist. Thus, the devices shown in Figs. 1 and 2 rotate endlessly.

Experiment: Fig. 3 shows experimentally obtained excess loss and phase difference of orthogonally polarised modes at an end facet of a single-mode fibre bent into a coil. The fibre was 125 μm in diameter with a cutoff wavelength of 1·41 μm and a relative index difference of 0·27%. It was silicone-coated with an outer diameter of 400 μm, and the wavelength was 1·52 μm. Fig. 3 indicates that, to reduce excess loss below